Three-Dimensional Instabilities in the Wake of a Circular Cylinder

Mark Thompson
Kerry Hourigan
John Sheridan
Department of Mechanical Engineering,
Monash University,
Clayton, Australia

■ The two- and three-dimensional wake structure behind a circular cylinder has been computed using a high-order spectral element technique. For the two-dimensional computations the predictions are compared with accurate experimental results and agree to within experimental uncertainty for the Strouhal number and base pressure coefficient. For the three-dimensional simulations, the two modes of three-dimensional instability, designated as modes A and B, both found experimentally but not previously computationally, have been captured. Mode A appears first at a Reynolds number slightly less than 200. As the Reynolds number is increased, there is a transfer of energy to mode B, which has a wavelength approximately one-fourth that of mode A.

Keywords: *bluff-body wakes, wake transition*

INTRODUCTION

Despite the fact that the flow past a circular cylinder has been studied for well over 100 years, and the geometrical configuration is a particularly simple one, this problem is still under intensive investigation today. Indeed, within the last 10 years, due to the efforts of many research groups (Williamson [1-3], Hammache and Gharib [4], Norberg [5], Eisenlohr and Ecklemann [6]), the experimental relationship between Strouhal and Reynolds numbers has been determined to within 1%, at least within the two-dimensional shedding regime. The previous discrepancies between different experimental teams seem to have stemmed from various factors including small aspect ratio cylinders, end effects, and oblique modes. The new "universal" results represent a challenge for computationalists who in the past have relied on the variation in experimental results to justify their predictions.

At a Reynolds number of approximately 180, the two-dimensional periodic Strouhal vortex wake undergoes a transition to three-dimensionality. This was observed by Roshko [7, 8] in the form of irregularities in the wake velocity fluctuations. Recent experiments undertaken by Williamson [1, 9] demonstrated that the transition to three-dimensionality involves two modes of formation of streamwise vorticity in the near wake. The two modes are dominant over different Reynolds number ranges.

When the wake first becomes three-dimensional, at Re $\approx$ 180 (Re $= 2u_\infty R/\nu$, where ν is the kinematic viscosity, R is the cylinder radius, and u_∞ is the free-stream velocity), mode A vortex shedding appears. This is characterized by regular streamwise vortices appearing in the wake, with a spanwise wavelength of approximately 3

cylinder diameters. At Re $\approx$ 230, a second mode (mode B) appears, consisting of a more irregular array of streamwise vortices with a mean spanwise wavelength of about 1 cylinder diameter. Between Re = 230 and Re = 260, there is a gradual redistribution of energy between the modes. At Re = 230, mode A dominates, while at Re = 260, mode B structures contain more energy. In this range both modes coexist. At each of these transitions, a discontinuity in the Strouhal number versus Reynolds number curve occurs. The appearance of mode A is hysteretic, while that of mode B is not.

Until recently there have been few numerical studies published on the three-dimensional wakes due to the significant computational resources required to properly resolve the flow structures. One investigation undertaken by Karniadakis and Triantafyllou [10] concentrated on the stability of the wake of a circular cylinder over a Reynolds number range up to 500 rather than a detailed study of the different modes that appear. The emphasis was on examining the route to fully turbulent flow followed by this (and similar) flows. Computational restrictions led them to use a fairly coarse mesh with a spanwise domain size that was too short to capture mode A. They suggest that the route to wake turbulence is via period-doubling.

In this paper, some preliminary results from numerical experiments examining both two- and three-dimensional flows are presented. The results of the simulations are compared with experimental results.

PROBLEM FORMULATION

The governing equations are the incompressible time-dependent Navier–Stokes equations in primitive variable

Address correspondence to Mark Thompson, Mechanical Engineering, Monash University, Clayton, Vic, 3168, Australia.

form. The equations are discretized using a time-split spectral/spectral element method as described by Karniadakis and Triantafyllou [10] and Tomboulides et al. [11] and references cited therein. Consequently only a brief overview is presented here.

Time-Stepping Scheme

The momentum equations are integrated forward in time by a three-step procedure. The steps account for the convection, pressure, and diffusion terms, respectively. The equation treating the convection term is treated explicitly because of its nonlinear nature. The equations for diffusion and pressure are treated implicitly. If memory is available, the matrices involved can be inverted in a preprocessing step. Otherwise, efficient iterative techniques for symmetric problems can be used (i.e., conjugate gradient methods). For the calculations described in this paper, only direct solvers were used.

The convection equation is integrated forward in time by the third-order Adams–Bashforth method, and the diffusion equation is treated by the Crank–Nicholson scheme. In the second step, the pressure is evaluated. A Poisson equation is formed by taking the divergence of the equation for the pressure substep, and continuity is enforced at the end of the substep. Second-order overall time accuracy is achieved by using a higher order pressure boundary condition as described in Karniadakis et al. [12].

Spatial Discretization

The spectral element technique [10] is employed for the two-dimensional (streamwise) flow (i.e., the xy planes). A typical (two-dimensional) spectral element mesh is shown in Fig. 1. It consists of $K = 60$ macroelements. Each element is mapped into a computational square, and high-order Lagrangian polynomial interpolants are used to approximate the solution variables in each direction. The Galerkin finite-element method is applied to form equations for the solution variables at the nodal points. The integrals of the flow equations multiplied by the local weighting functions are (approximately) evaluated by Gauss–Legendre–Lobatto quadrature. This approach is particularly economical computationally in that only a limited number of element nodes contribute to the equations formed at a particular node. For example, the "mass"

matrix is diagonal in this case; this would not occur if Gauss–Legendre quadrature was used, for example. Further economy is gained by using static-condensation techniques. This method relies on the fact that the equations for the internal nodes of each element depend only on the boundary nodes, and hence the matrix equations can be decoupled into two sets, one involving the element boundary nodes and the other, K small matrix equations for the internal nodes of each element. The latter K equations can be evaluated after the first (larger) matrix equation is solved. A bandwidth minimization scheme can reduce the bandwidth (and hopefully overall size) of the matrices, and sparse matrix solvers are used to solve the large systems of equations involved. Due to the form of the splitting scheme, the matrix inversions need to be performed only at the beginning of the calculations.

A Fourier spectral discretization is employed in the spanwise direction. This has significant computational benefits. The equations for each Fourier mode decouple, leading to small matrix equations for each mode rather than a large coupled matrix equation with a large bandwidth that would be much more computationally expensive. An efficient implementation can be achieved on parallel architecture machines due (in part) to this decoupling. For the work described here, though, the computations were performed in double precision on a serial Silicon Graphics workstation rated at about 12 megaflops with 12 megawords of main memory.

TWO-DIMENSIONAL STUDIES

As mentioned previously, experimental studies indicate that the wake becomes three-dimensional at a Reynolds number of ~ 180. Two-dimensional simulations below this Reynolds number should adequately reproduce the results of experimental measurements that are believed to be within 1% for the Strouhal number [2, 13]. At higher Reynolds numbers, two-dimensional computations can provide a comparison for three-dimensional computations and experiments.

Strouhal Number

In previous computational studies, an often-quoted test of accuracy for cylinder flow computations has been the variation of Strouhal number with Reynolds number.
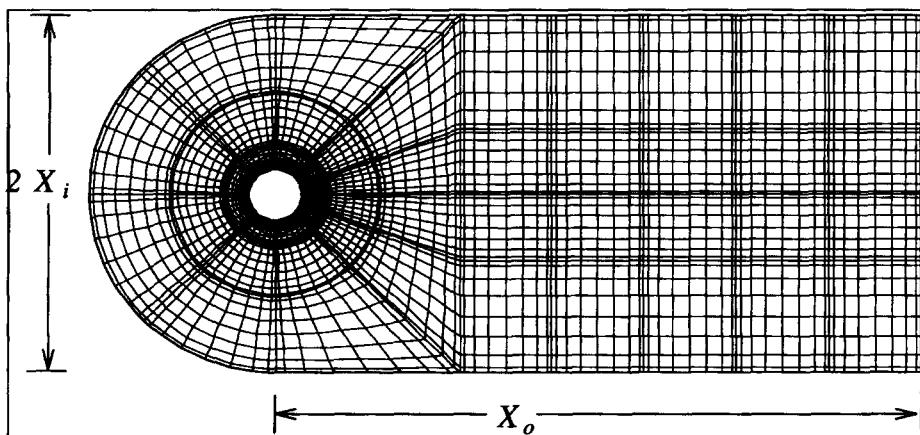
Figure 1. Two-dimensional view of three-dimensional mesh system showing the spectral element discretization. This mesh has $K = 60$ elements.

Williamson [2,13] has given a least-squares fit to the universal Strouhal number curve for the low Reynolds number regime as

$$St = \frac{A}{Re} + B + C\,Re, \tag{1}$$

where $A = -3.3265$, $B = 0.1816$, and $C = 0.00016$.

The three-dimensional computations require a considerable amount of CPU time and memory, and hence for this preliminary study at least, the three-dimensional runs were done on a *small* mesh. The aim of this section is to verify that the computational scheme can reproduce two-dimensional experimental results to within experimental error and to establish the effect of using a domain smaller than desirable.

Karniadakis and Triantafyllou [10] found in their numerical experiments that, over a limited number of tests, the Strouhal number (1) increased with decreasing inflow length, (2) was insensitive to the outflow length (between 36 and 70 cylinder radii), and (3) increased with decreasing domain width. They also confirmed that the level of resolution they used was sufficient by showing that increasing the resolution per element did not affect the Strouhal number.

The domain is described by three main parameters: the number of elements (K), inflow length and domain width (X_i), and outflow length (X_o). In addition, the distribution of elements within the domain also will strongly influence the overall accuracy of the results. The mesh used for the three-dimensional calculations is shown in Fig. 1. This has $X_i = 7R$ and $X_o = 24.5R$. Some larger meshes were used to try to reproduce the two-dimensional results as accurately as possible. This mesh (with $K = 60$ elements) was used as a basis together with either or both (1) an *expandable* layer of elements to extend the inflow length and domain width and (2) elements extending the outflow length.

The effect of the number of nodes per element in each direction (N) is shown in Table 1. (Note that the order of the interpolating polynomial is $N - 1$.) For a calculation at Re = 200 on the mesh shown in Fig. 1, the Strouhal number has converged to better than 0.1% by $N = 9$.

The Strouhal number is sensitive to the size of the domain. An accurate determination (to within the error in the experimental values) requires the outer boundary to be placed approximately $30R$ from the cylinder. The inflow and outer boundary conditions will obviously affect this conclusion. For the present computations, the inflow and outer boundary conditions are taken from the potential flow solution. Also, the outflow boundary conditions

Table 1. Dependence of Strouhal Number on Polynomial Order for Small Mesh at Re = 200 for a Constant Time Step of 0.01[a]

Element Size ($N \times N$)	Strouhal Number
5 × 5	0.2036
7 × 7	0.2101
9 × 9	0.2107
11 × 11	0.2107
13 × 13	0.2108

[a] Two-dimensional simulation.
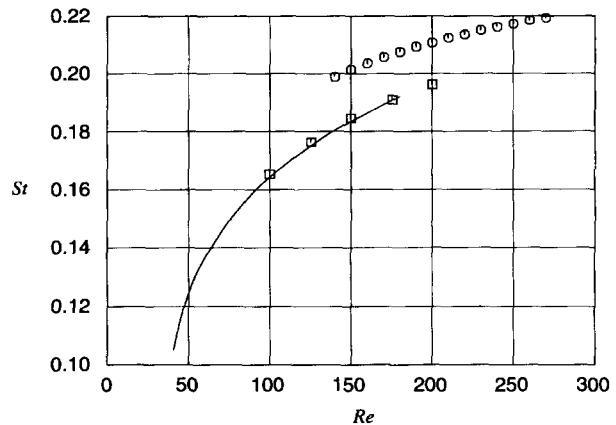
Figure 2. Variation of Strouhal number with Reynolds number. The square symbols indicate results for large domain (106 [9 × 9] elements, $X_i = 50R$, $X_o = 42.5R$), and the rounded symbols are for the small mesh used for the 3D calculations (60 [9 × 9]) elements. The solid curve is the experimental fit given in [13].

are taken to be $\partial v/\partial n = 0$ and $p = 0$. For all these runs the shedding becomes truly periodic at the Strouhal frequency, with no other identifiable frequency components.

Figure 2 shows computations of the St-Re relationship for two different mesh systems: the mesh shown in Fig. 1 (round symbols) and a mesh corresponding to a larger domain ($X_i = 50R$, $K = 106$, $X_o = 42.5R$) (square symbols). Each mesh has 9 × 9 nodes per element. The curve of best fit to the experimental data, given by Eq. (1), is shown for comparison. The results for the large domain are within 1% of the experimental values for the two-dimensional shedding range. (Strouhal numbers were calculated for a series of meshes with different X_i up to $50R$. Extrapolation indicates that the Strouhal number for the mesh with $X_i = 50R$ is within about 0.5% of the infinite domain width result.) For the smaller mesh, the results are within about 7%. Calculations were done for several meshes of intermediate size to ensure that the results for the large domain are close to the asymptotic result. It is believed that the restricted domain should not alter the essential physics underlying the development and interaction of the three-dimensional structures although it might influence variables such as the Reynolds number at which three-dimensionality first occurs.

Other Tests

Although spectral element/spectral methods possess the property of exponential convergence (i.e., converging faster than any power of the number of nodes), in practice this asymptotic convergence rate may have little relevance. Unless the number of nodes per element is large enough that flow features can be resolved by the functional representation, these methods can be worse than using much lower order methods. A recent case in point is found in Kaiktsis et al. [14], which presents results for flow past a backward-facing step and predicts unsteady behavior at Re = 800. This prediction appears to be a result of inadequate resolution. Most other computations using different methods indicate that the flow is steady, and calculations

using a very similar spectral element code with more nodes per element also indicate a steady flow [15].

The Strouhal number may not be a very sensitive indicator that a particular mesh system has sufficient resolution to adequately resolve the flow field. It may, for instance, depend more on the grid resolution in the neighborhood of the cylinder and not the downstream resolution. An alternative test is to look at the variation of the velocity field at a point some distance downstream of the cylinder. Figure 3 shows the dependence of the extremes of the u component of the velocity on the element order N. These values are taken at a point $7R$ downstream of the cylinder at Re = 200. Clearly, the curves are beginning to flatten out at $N = 9$.

As a final validation, the base pressure coefficient

$$C_{pb} = (p - p_\infty)/(1/2\rho u_\infty^2)$$

was computed for several Reynolds numbers and compared with the experimental measurements of Williamson and Roshko [16]. The predictions are approximately 2–3% below the measurements for parallel shedding for the Reynolds number range 100–180. The base pressure coefficient is much more difficult to measure accurately than is the Strouhal number, and the discrepancies between sets of experimental data are considerably greater [5, 16].
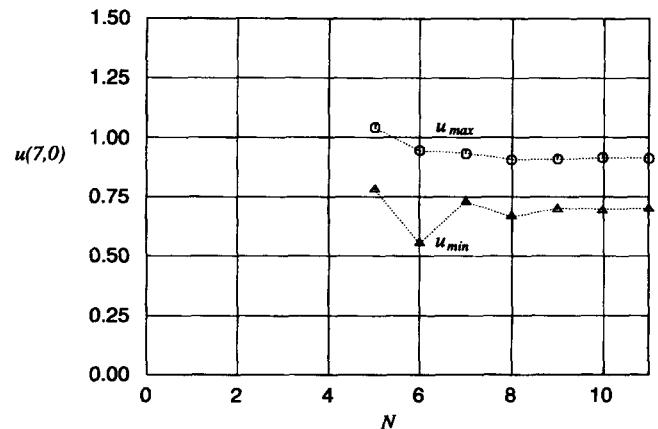
Figure 3. Dependence of the extremes of $u(7,0)$ on polynomial order N for the $K = 60$ element mesh at Re = 200.

THREE-DIMENSIONAL SIMULATIONS

Numerical simulations of the onset of three-dimensionality have been reported previously by Karniadakis and Triantafyllou [10] and Tomboulides et al. [11]. In their studies, emphasis was placed on the stability analysis and transition to turbulence. In the current study, the focus is on the appearance of the two three-dimensional instability
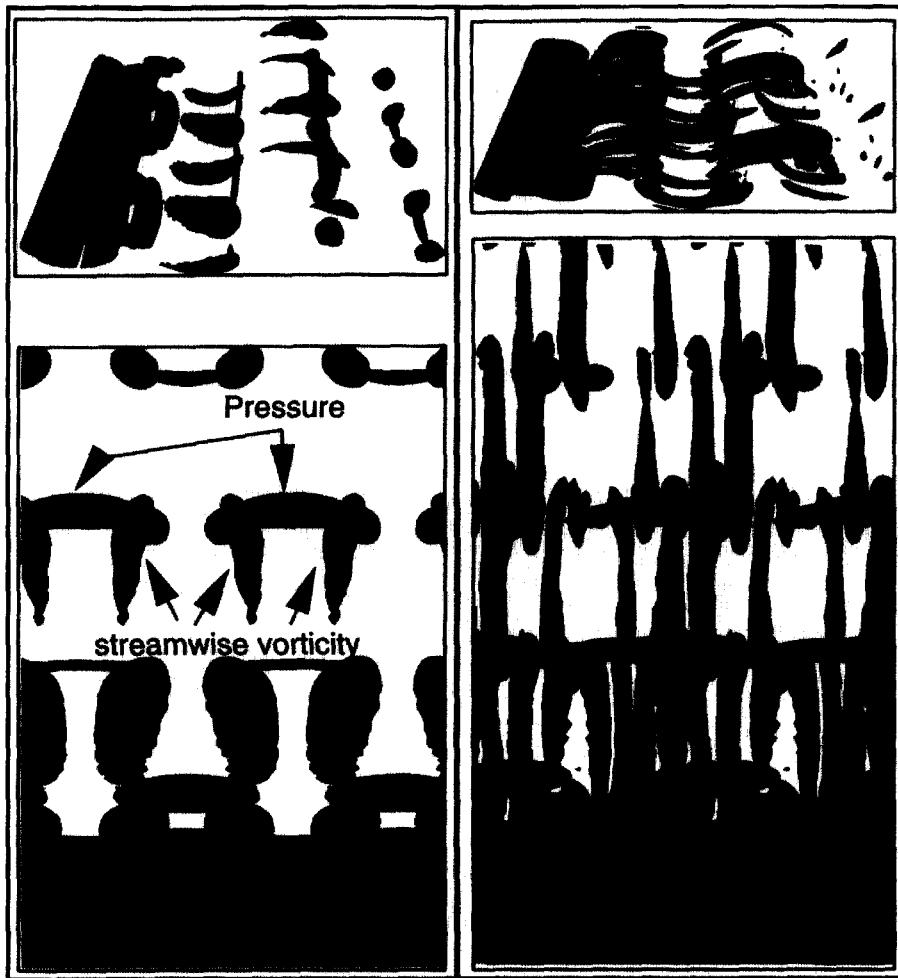
Figure 4. Alternative views of isosurfaces of pressure ($p = -0.4$, black) and streamwise vorticity ($\omega_x = \pm 0.4$). The cylinder is also shown (light gray). The views on the left are for Re = 200 (mode A shedding), and those on the right for Re = 250 (mode B shedding). The top diagrams are perspective views with the flow from left to right. The bottom diagrams show (orthographic) plan views of the two shedding modes, for which the flow is from the bottom to the top. The pressure isosurfaces mark the position of the predominantly two-dimensional spanwise Strouhal vortices. For reasons of clarity, the cylinder span length displayed is $4\pi R$, twice the computational span length.

modes, A and B, and the redistribution of energy between the two modes as the Reynolds number is increased. The topology of the three-dimensional structures is also examined.

Simulation at Re = 250

To investigate the development of the three-dimensional instability, a computation was performed at Re = 250, with 24 Fourier terms and a spanwise periodicity length of $2\pi R$. This span length was chosen from the observations of Williamson [1], who measured the spanwise wavelength for mode A to be approximately $6R$. The computation was started from the periodic field taken from a two-dimensional simulation. The initially zero w velocity component was perturbed by a random amount at each point (at a level of 10^{-4}) to accelerate development of the three-dimensionality. After six Strouhal shedding cycles, plots of isosurfaces of the streamwise vorticity clearly show the appearance of coherent three-dimensional structures with a spanwise wavelength of $2\pi R$. The magnitude of the streamwise vorticity is very low at this time. The maximum value over the field is about 0.02. After 15 cycles, the structures are much stronger still with a wavelength of $6R$. At 25 cycles, the structures have almost reached maximum strength [$\max(\omega_{st} \equiv \sqrt{\omega_x^2 + \omega_y^2}) \approx 3$]. There also appears to be some finer scale structure developing at this time.

After about 40 Strouhal periods from initiation of the three-dimensional disturbance, the three-dimensional structures change in character. Figure 4 (right) shows the isosurfaces at that time. The spanwise wavelength has been reduced to $\pi/2R$. This is more typical of the mode B shedding observed experimentally.

The simulation was continued for approximately 100 Strouhal cycles and did not show any sign of reaching a steady periodic state. The u and w velocity traces at (1.88, -0.69) are shown in Fig. 5. (The Strouhal period is approximately 10.) There is no obvious indication of the period doubling found by Karniadakis and Triantafyllou [10] and Tomboulides et al. [11], who used a span length of only half of that used for the present simulations and therefore could not resolve mode A. Computations using the smaller spanwise domain (πR) do indicate period doubling at this Reynolds number, in line with the results from these papers. It is not clear whether the period doubling exists when the two modes are present together. Indeed, to some extent, at this Reynolds number it appears that the three-dimensional structures seem to alternate between the two different modes. This is consistent with the experimental findings for the transition region

between the two shedding modes. In this Reynolds number range (230 < Re < 260), experimental results show two peaks in the frequency spectrum, presumably corresponding to the coexistence of the two modes [2].

Simulation at Other Reynolds Numbers

A computation at Re = 200 was carried out starting from a fully developed three-dimensional velocity field from the simulation at Re = 250. After a transition period, the velocity field settles down to a periodic state corresponding to mode A shedding. A simulation at Re = 210 gives a similar result, but in this case the streamwise vortex structures are more pronounced.

Visualization of the Three-Dimensional Structures

The two different shedding modes are characterized in Fig. 4. The different views show isosurfaces of streamwise vorticity ($\omega_x = \pm 0.4$, dark gray), isosurfaces of pressure ($p = -0.4$, black) and the position of the cylinder (light gray). The pressure isosurfaces mark the position of the Strouhal vortices. The visualizations on the left show the mode A shedding pattern at Re = 200. Similar visualizations for the mode B shedding regime at Re = 250 are shown on the right. The cylinder section displayed is twice the actual computational domain span length. The spanwise wavelength is $2\pi R$, which is close to the experimentally observed wavelength for mode A shedding.

At Re = 200 (close to the onset of mode A shedding), the strength of the streamwise vortex structures is about half of the peak vorticity of the Strouhal vortices in the near wake. The peak streamwise vorticity is approximately $1\,u_\infty/R$ unit, while the vorticity in the spanwise vortex structures is approximately 2. These numbers will vary with position and should be taken as only a guide to the relative magnitudes. At Re = 250, in the mode B shedding regime, the measured peak vorticity was similar for the streamwise and spanwise structures at typically 2 u_∞/R units.

These isosurface plots demonstrate the main features of the two shedding modes. Mode A shedding is periodic, with the streamwise vortex structures aligned from one Strouhal cycle to the next. Mode B shedding is less regular, with less alignment of the vortices. For that mode the streamwise vortex structures are not all of the same strength and can grow or decay relative to their neighbors as they move downstream. The difference in spanwise wavelength between the two shedding modes is clearly visible.

As a comparison, experimental visualizations of the two modes are shown in Fig. 6. The picture on the left shows
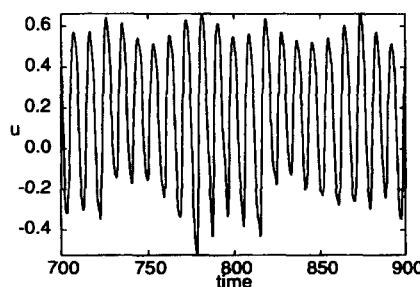
Figure 5. Time evolution of the u (left) and w (right) velocity components at position (1.88, -0.69) at Re = 250.
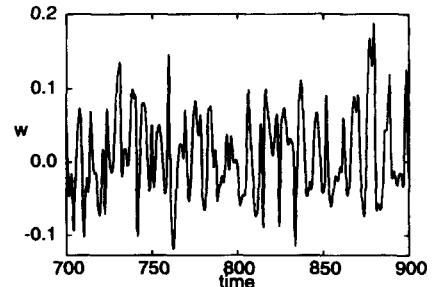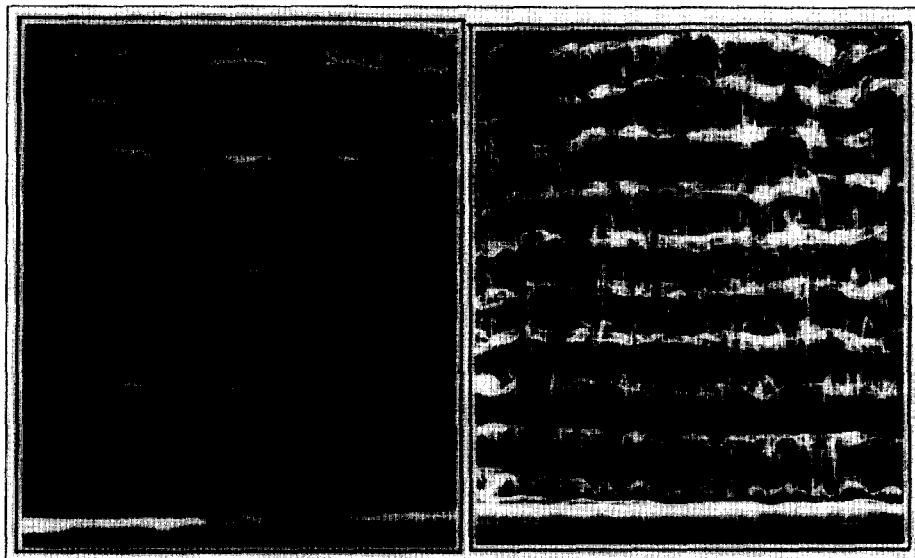
Figure 6. Experimental visualizations using fluorescein dye and laser light of the two shedding modes. The picture on the left shows mode A shedding for Re = 200, and the one on the right is typical of mode B shedding. The latter is for Re = 285 and is representative of patterns observed for Re ≥ 230. (Visualizations courtesy of C. H. K. Williamson.)

the mode A streamwise structures at Re = 180, and the one on the right is a similar depiction for mode B shedding at Re ≥ 230, both to the same scale. These flows were visualized with laser light, and fluorescein dye washed off the cylinder as it was towed along a (towing) tank. Obviously, streamwise vortex structures cannot be directly compared with dye visualizations; however, the experimental and computational results appear to be consistent for each mode in a number of features. In particular, the different visualizations are similar in the spanwise wavelength of the streamwise vortex "loops" for each mode and in the regularity (for mode A) and decrease in regularity (for mode B) of the structures from one cycle to the next.

Effect of Span Length

To test the preferred spanwise wavelength of mode A, a computation was performed with a domain span length of $4\pi R$ and 48 Fourier terms at Re = 250. As before, a perturbed two-dimensional velocity field was used to begin the simulation. The results were similar to those found with the narrower domain, with the mode A wavelength again equal to $2\pi R$.

Effect on Base Pressure Coefficient

Table 2 shows the effect of the three-dimensional shedding on the base pressure coefficient for the 60-element mesh. The values are affected by blockage due to the narrowness of the domain, but the relative difference between the two- and three-dimensional results is signifi-

Table 2. Effect of Three-Dimensional Shedding on the Base Pressure Coefficient for the Mode A Reynolds Number Range

Reynolds Number	2D Base Pressure Coefficient	3D Base Pressure Coefficient
190	−1.252	−1.252
200	−1.270	−1.250
210	−1.289	−1.219

cant. At Re = 210, the base pressure coefficient is about 6% less than the prediction from the two-dimensional simulation. The decrease in base pressure suction is consistent with the experimental results of Williamson and Roshko [16] and Norberg [5].

PRACTICAL SIGNIFICANCE / USEFULNESS

Recent comparisons of two- and three-dimensional computations of flows past bluff bodies indicate that only the three-dimensional computations produce acceptable predictions of the aerodynamic forces [17]. However, three-dimensional simulations are very demanding of computational resources and are presently possible only for low Reynolds numbers and simple body shapes. One aim of the present work is to eventually be able to investigate the physics underlying the three-dimensional flow structures to understand their role in modifying aerodynamic quantities such as lift and drag.

As a first step in this task it is important to verify computations against available experimental observations and data. The predictions of the current computations do seem to satisfy this requirement. It is anticipated that a better understanding of the physics behind these flows will result from the interaction of experimental and computational research.

An important application of this and further research will be in predicting pressure coefficients and lift and drag coefficients of bluff bodies. It is found that fully resolved two-dimensional simulations do not produce accurate pressure distributions for flows once they become three-dimensional [10]. This is consistent with the current set of results, which show that once the shedding becomes three-dimensional the base pressure coefficient from three-dimensional simulations deviates considerably from the two-dimensional prediction.

CONCLUSIONS

Three-dimensional simulations of the flow past an infinite, two-dimensional circular cylinder show features similar to those found experimentally. In particular, the computa-

tions predict the two shedding modes that occur for different Reynolds number ranges and give spanwise wavelengths consistent with the experimental values. There are indications that the two modes can coexist for intermediate Reynolds numbers (i.e., Re = 250), which is also consistent with experiments.

Computations are currently under way using larger and more refined meshes to try to understand the transition process more fully.

NOMENCLATURE

K number of (spectral) elements, dimensionless

N number of nodes in each direction in an element, dimensionless

R cylinder radius, (m)

Re   Reynolds number ($\equiv 2u_\infty R/\nu$), dimensionless

St   Strouhal number ($\equiv 2fR/u_\infty$), dimensionless

X_i domain inflow length, (m)

X_o domain outflow length, (m)

f vortex shedding frequency (5^{-1})

p pressure, (N/m^2),

u_∞ free-stream velocity, (m/s)

v fluid velocity, (m/s)

Greek Symbols

ν kinematic viscosity, (m^2/5)

ω vorticity (5^{-1}),

ω_{st} two-dimensional vorticity magnitude, (5^{-1})

ω_x streamwise vorticity component, (5^{-1})

ρ fluid density, (Kg/m^3)

REFERENCES

1. Williamson, C. H. K., The Existence of Two Stages in the Transition to Three-Dimensionality of a Cylinder Wake, *Phys. Fluids* **31**, 3165, 1988.
2. Williamson, C. H. K., 2-D and 3-D Aspects of the Wake of a Cylinder, and Their Relation to Wake Computations, *Lect. Appl. Math.* **28**, 719-751, 1991.
3. Williamson, C. H. K., Three-Dimensional Aspects and Transition of the Wake of a Circular Cylinder, in *Turbulent Shear Flows, Vol.*

7 (F. Durst, B. E. Launder, W. C. Reynolds, F. W. Schmidt, and J. H. Whitelaw, Eds.), pp. 173-194, Springer-Verlag, New York, 1991.
4. Hammache, M., and Gharib, M., A Novel Method to Promote Parallel Vortex Shedding in the Wake of a Circular Cylinder, *Phys. Fluids* **A1**, 1611-1614, 1989.
5. Norberg, C., An Experimental Investigation of the Flow Around a Circular Cylinder: Influence of Aspect Ratio, *J. Fluid Mech.* **258**, 287, 1994.
6. Eisenlohr, H., and Eckelmann, H., Vortex Splitting and Its Consequences in the Vortex Street Wake of Cylinders at Low Reynolds Numbers, *Phys. Fluids* **A1**, 189, 1989.
7. Roshko, A., On the Development of Turbulent Wakes from Vortex Streets, NACA Rep. 1191, 1954.
8. Roshko, A., On the Wake and Drag of Bluff Bodies, *J. Aerosp. Sci.* **22**, 124-132, 1955.
9. Williamson, C. H. K., The Natural and Forced Formation of Spot-Like "Vortex Dislocations" in the Transition of a Wake, *J. Fluid Mech.* **243**, 393-441, 1992.
10. Karniadakis, G. E., and Triantafyllou, G. S., Three-Dimensional Dynamics and Transition to Turbulence in the Wake of Bluff Objects, *J. Fluid Mech.* **238**, 1-30, 1992.
11. Tomboulides, A. G., Triantafyllou, G. S., and Karniadakis, G. E., A New Mechanism of Period Doubling in Free Shear Flows, *Phys. Fluids* **4**, 1329-1332, 1992.
12. Karniadakis, G. E., Israeli, M., and Orszag, S. A., High-Order Splitting Methods for the Incompressible Navier-Stokes Equations, *J. Comp. Phys.* **97**, 414-443, 1991.
13. Williamson, C. H. K., Defining a Universal and Continuous Strouhal-Reynolds Number Relationship for the Laminar Vortex Shedding of a Circular Cylinder, *Phys. Fluids* **31**, 2742, 1988.
14. Kaiktsis, L., Karniadakis, G. E., and Orszag, S. A., Onset of Three-Dimensionality, Equilibria, and Early Transition in Flow over a Backward Facing Step, *J. Fluid Mech.* **231**, 501-528, 1991.
15. Gresho, P. M., Gartling, D. K., Torczynski, J. R., Cliffe, K. A., Winters, K. H., Garratt, T. J., Spence, A., and Goodrich, J. W., Is the Steady Viscous Incompressible Two-Dimensional Flow over a Backward-Facing Step at Re = 800 Stable?, *Int. J. Numer. Methods Fluids* **17**, 501-541, 1993.
16. Williamson, C. H. K., and Roshko, A., Measurements of Base Pressure in the Wake of a Cylinder at Low Reynolds Numbers, *Z. Fluggwiss. Weltraumforsch.* **14**, 38-46, 1990.
17. Tamura, T., Ohta, I., and Kurahara, K., On the Reliability of Two-Dimensional Simulation for Unsteady Flows Around a Cylinder Type Structure, *J. Wind Eng. Ind. Aerodyn.* **35**, 275-298, 1990.